

Static stress transfer during the 2002 Nenana Mountain-Denali Fault, Alaska, earthquake sequence

Greg Anderson

U.S. Geological Survey, Pasadena

Chen Ji

Seismological Laboratory, California Institute of Technology

Abstract. On 23 October 2002, the M_w 6.7 Nenana Mountain earthquake occurred in central Alaska. It was followed on 3 November 2002 by the M_w 7.9 Denali Fault mainshock, the largest strike-slip earthquake to occur in North America during the past 150 years. We have modeled static Coulomb stress transfer effects during this sequence. We find that the Nenana Mountain foreshock transferred 30–50 kPa of Coulomb stress to the hypocentral region of the Denali Fault mainshock, encouraging its occurrence. We also find that the two main earthquakes together transferred more than 400 kPa of Coulomb stress to the Cross Creek segment of the Totschunda fault system and to the Denali fault southeast of the mainshock rupture, and up to 80 kPa to the Denali fault west of the Nenana Mountain rupture. Other major faults in the region experienced much smaller static Coulomb stress changes.

1. Introduction

The 2002 Nenana Mountain-Denali Fault earthquake sequence occurred along the Denali fault, a major strike-slip fault system in central Alaska which slips right-laterally in response to oblique subduction of the Pacific Plate under North America (Figure 1). The 23 October 2002 M_w 6.7 Nenana Mountain (NM) foreshock (Alaska Earthquake Information Center hypocenter: 63.5144°N, 147.9116°W, 4.2 km depth) was the largest earthquake known to have occurred on the Denali fault since at least 1912. It was followed on 3 November 2002 by the M_w 7.9 Denali Fault (DF) mainshock (AEIC hypocenter: 63.5175°N, 147.4440°W, 4.9 km depth), which was the largest North American strike-slip earthquake since the 1857 Fort Tejon event in southern California. The DF mainshock was much more complex than the NM foreshock, rupturing about 290 km of the Denali and Totschunda faults, and about 40 km of the newly-discovered Susitna Glacier fault (SGF), with a mixture of oblique thrust and right-lateral motion. The maximum observed surface offsets were about 8.8 meters [P. Haeussler *et al.*, Surface rupture of Alaska’s magnitude-7.9 earthquake in November 2002, submitted to *Science*, 2003]. The close proximity of the NM and DF earthquakes suggests a possible link between them, which we investigate by modeling Coulomb stress transfer from the

NM foreshock to the DF mainshock. We also examine the combined effect of the NM and DF events on several major regional faults.

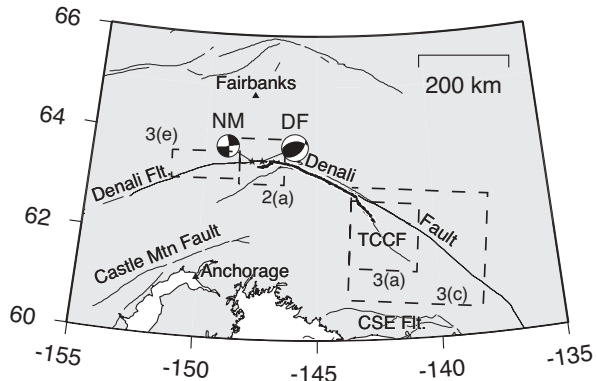


Figure 1. Location map of central Alaska. First-motion focal mechanisms for the Nenana Mountain (NM) and Denali Fault (DF) earthquakes were determined by the AEIC from local and regional seismograms. Boxes show areas covered by smaller maps in Figures 2(a), 3(a), 3(c), and 3(e). Denali, Castle Mountain, Totschunda-Cross Creek (TCCF), and Chugach-St. Elias (CSE Flt) faults are labeled. Heavy line indicates the DF mainshock surface rupture.

2. Coulomb stress change modeling

We represent the NM and DF sources using finite-fault slip models derived by *Ji et al.* [2002] from teleseismic waveform modeling. Given these models, we use the theory of elastic deformation from dislocations in a half-space [Okada, 1992] to compute coseismic stress increment tensors at specific locations. We resolve these tensors into Coulomb stress change on faults of specified strike, dip, and rake; the change in Coulomb stress is given by [Reasenber and Simpson, 1992; Simpson and Reasenber, 1994]

$$\Delta\text{CFF} = \Delta\tau + \mu' \Delta\sigma, \quad (1)$$

where $\Delta\tau$ is the coseismic change in shear stress in the direction of fault slip, $\Delta\sigma$ is the change in normal stress (with tension positive), and μ' is the effective coefficient of friction, accounting for pore-fluid pressure effects. For this work, we use $\mu' = 0.4$ and we perform all calculations using an elastic halfspace with Poisson's ratio of 0.25 and a shear modulus of 30 GPa.

3. Effect of NM foreshock on DF mainshock

We first examine Coulomb stress transferred from the NM event to the hypocentral region of the DF mainshock. The AEIC hypocenter for the DF earthquake is located south of the main Denali fault, and the first-motion focal mechanism determined by the AEIC from local and regional seismograms is consistent with oblique thrust motion (115° rake) on a fault striking N262E and dipping 48° to the north-northwest. These data indicate that the DF earthquake began as an oblique thrust event on the SGF, and we therefore model Coulomb stress transfer from the NM foreshock to the SGF.

Field investigations [P. Haeussler *et al.*, submitted to *Science*, 2003] show that the shallow SGF dips $\leq 25^\circ$, while the AEIC focal mechanism indicates the deeper SGF dips $> 45^\circ$. We are interested primarily in the effect of the NM event on DF event initiation, and therefore in estimating stress change on the SGF in the more steeply-dipping region near the hypocenter. Accordingly, we model the DF mainshock hypocentral region as a plane consistent with the AEIC focal mechanism, centered on the AEIC hypocenter, that is 10 km long in the down-dip direction and 20 km long in the along-strike direction. To estimate the effect of hypocentral location uncertainty on our results, we also compute stress increment tensors on a 100x100 km horizontal grid surrounding the AEIC epicenter, with 0.5 km grid spacing and at depths of 5, 10, and 15 km. We resolve these tensors into ΔCFF on planes parallel to, and with the same sense of slip as, our model hypocentral plane.

Figure 2(a) shows a map view of ΔCFF at the 5 km hypocentral depth of the DF mainshock, and Figure 2(b)

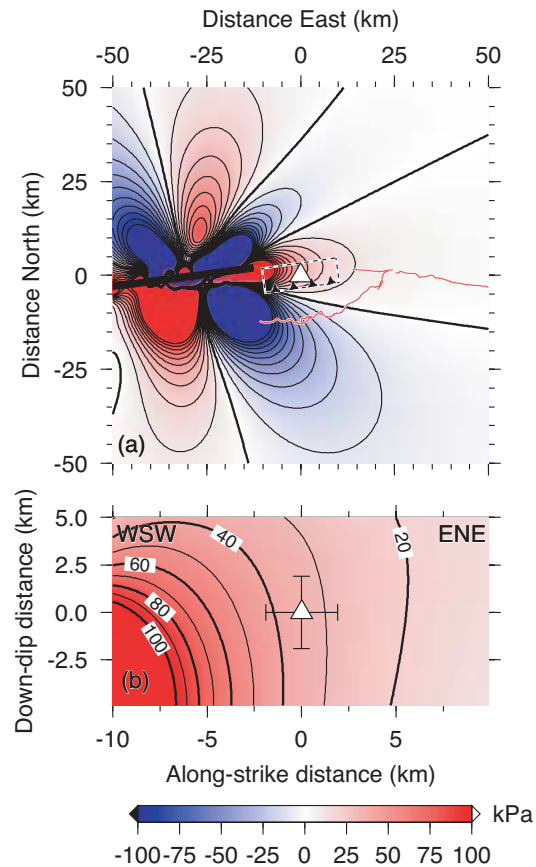


Figure 2. (a) Map view of ΔCFF at 5 km depth, for planes parallel to our model SGF rupture plane. Open triangle: AEIC DF event epicenter. Dashed rectangle: surface projection of our SGF model plane. Solid rectangles: surface projection of the *Ji et al.* [2002] NM model. Red line: DF event rupture surface trace. Distances are relative to the AEIC epicenter for the DF event. (b) Fault-parallel cross section of ΔCFF on our model SGF rupture plane. Open triangle: AEIC hypocenter for DF; error bars represent one standard deviation. In both subfigures, red indicates positive ΔCFF , encouraging rupture, and blue indicates negative ΔCFF . Contour interval is 10 kPa and distances are relative to the AEIC DF event hypocenter.

shows a fault-parallel cross section of ΔCFF . We find the NM event induced 30–50 kPa of positive Coulomb stress change on the hypocentral region of the DF earthquake; the range indicates uncertainty in ΔCFF due to the uncertainty in hypocentral location and other parameters. Numerous studies of stress transfer [e.g., *Harris*, 1998; *Stein*, 1999, and references therein] have indicated that ΔCFF levels of 10–20 kPa are associated with significant triggering of aftershocks and regional seismicity, and if these observations hold for faults in central Alaska, our results indicate the NM foreshock may have significantly

advanced the rupture time of the DF mainshock.

4. Combined effect of NM and DF events on regional fault systems

We next examine the combined effect of the NM and DF events on several major regional faults, including the unruptured segments of the Denali and Totschunda-Cross Creek fault systems, the large, oblique right-lateral thrust Castle Mountain fault near Anchorage, and the Chugach-St. Elias fault and Yakataga subduction interface associated with the collision of the Yakutat terrane with southern Alaska. We model each target fault segment as a single plane with the parameters listed in Table 1 and compute the combined ΔCFF generated by the NM and DF events on the target plane, using the same μ' , Poisson's ratio, and shear modulus as we used in the previous section. We also compute stress increment tensors on horizontal grids surrounding each target fault, at 5, 10, and 15 km depths, and resolve these tensors into ΔCFF on planes parallel to, and with the same sense of slip as, each target fault.

Of the segments listed in Table 1, our planes representing the northwestern segment of the Cross Creek fault (CCNW), the segment of the Denali fault immediately southeast of the DF earthquake rupture (DSE1), and the Muldrow segment of the DF, west of the NM rupture, experienced particularly large stress changes. Figures 3(a), 3(c), and 3(e) show map views of ΔCFF at 5 km depth for faults parallel to, and with the same sense of slip as, our CCNW, DSE1, and Muldrow planes, respectively. Figures 3(b), 3(d), and 3(f) show cross sections of ΔCFF on those planes. The CCNW plane was loaded during the NM-DF sequence by up to 420 kPa (the small areas of negative ΔCFF at depth on the cross section are artifacts of the proximity of our CCNW plane to the DF rupture model), while our DSE1 plane was loaded by up to 470 kPa, and our Muldrow plane was loaded by as much as 80 kPa.

The remaining faults in Table 1 experienced smaller stress changes, though in some cases marginally significant based on the 10–20 kPa threshold. The maximum estimated ΔCFF values on the DF segment southeast of DSE1 (DSE2) and the Yakataga subduction interface are 20 and -20 kPa, respectively, and on the southeastern Cross Creek fault (CCSE) and the Castle Mountain fault, the maximum values are 10 and -10 kPa. However, while these peak values are marginally significant, ΔCFF over most of the area of these faults is insignificant. The Tonzona and Boss Creek segments of the Denali fault (west of the Muldrow segment) and the Chugach-St. Elias fault were essentially unaffected by this sequence, experiencing ΔCFF of less than 6 and -8 kPa, respectively.

5. Conclusions

We have modeled static Coulomb stress transfer effects during the 2002 Nenana Mountain-Denali Fault, Alaska, sequence. We find the Nenana Mountain foreshock transferred 30–50 kPa of Coulomb stress to the hypocentral region of the Denali Fault mainshock, encouraging its subsequent failure. We also find that the NM and DF events together transferred more than 400 kPa of Coulomb stress to the northwestern Cross Creek segment of the Totschunda fault system and to the Denali fault southeast of the DF mainshock rupture; they also loaded the Denali fault west of the NM rupture by up to 80 kPa.

These stress changes are much larger than the 10–20 kPa ΔCFF levels often associated with significant changes in regional seismicity patterns following large earthquakes. Our results thus suggest that the NM-DF sequence should have significantly advanced the time of the next earthquake on each segment. Because each segment has a poorly-known history of prior earthquakes and a different unknown background stress state, we cannot state with any confidence which of these segments is most likely to rupture next, but as a group, these segments merit careful attention as possible sources for significant future earthquakes.

Acknowledgments.

We used Bob Simpson's DLC and GCLR codes for our stress transfer modeling, and we thank Bob for answering multiple questions via e-mail and on the phone. Art Tarr provided us with digitized versions of the *Plafker et al.* [1994] DNAG Alaska fault map. We want to thank Brad Aagaard, Patty Craw, Donna Eberhart-Phillips, Jeff Freymueller, Gary Fuis, Peter Haeussler, Ruth Harris, Lucy Jones, Nancy King, Bob Page, Liz Smith, Ross Stein, and Chris Zweck for data and suggestions, and Brad Aagaard, Ruth Harris, Sue Hough, Debbie Liang, David Oglesby, and an anonymous reviewer for critical reviews which improved this manuscript. We plotted some figures using the Generic Mapping Tools (GMT) [*Wessel and Smith, 1998*].

References

- Harris, R. A., Introduction to special section: Stress triggers, stress shadows, and implications for seismic hazard, *J. Geophys. Res.*, 103, 24,347–24,358, 1998.
- Ji, C., D. Helmberger, and D. Wald, Preliminary slip history of the 2002 Denali earthquake, *EOS Trans. AGU*, 83, 2002, Abstract S72F-1344.
- Lahr, J. C., R. A. Page, C. D. Stephens, and K. A. Fogleman, The Sutton, Alaska, earthquake of 1984: Evidence for activity on the Talkeetna segment of the Castle Mountain fault system, *Bull. Seismol. Soc. Am.*, 76, 967–983, 1986.
- Okada, Y., Internal deformation due to shear and tensile faults in a half-space, *Bull. Seismol. Soc. Am.*, 82, 1018–1040, 1992.
- Plafker, G., L. Gilpin, and J. C. Lahr, Neotectonic map of Alaska, in *The Geology of Alaska*, edited by G. Plafker

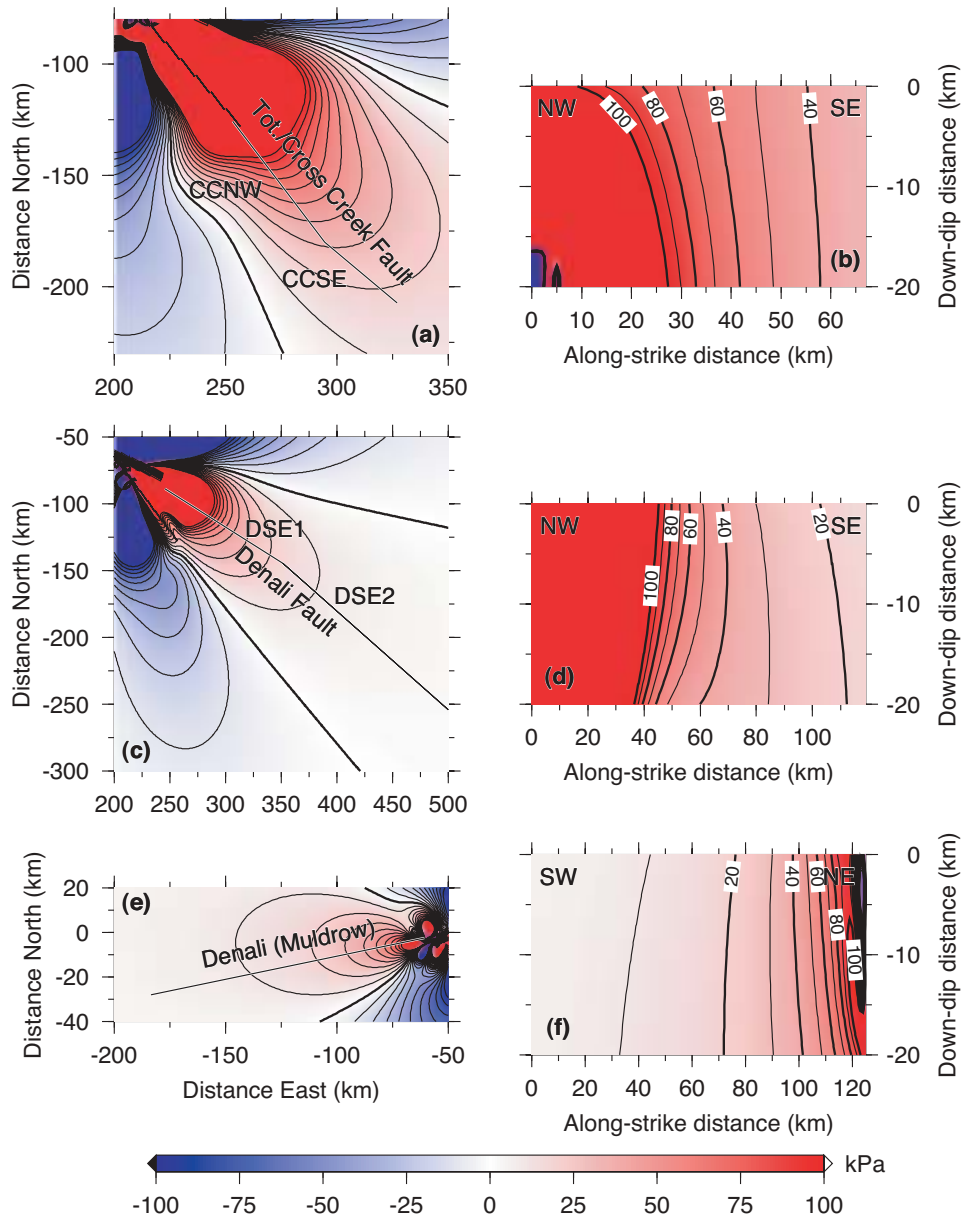


Figure 3. (a) Map view of ΔCFF at 5 km depth, for planes parallel to and with the same sense of slip as our CCNW plane. (b) Fault-parallel cross section of ΔCFF on our CCNW plane. (c) Same as (a), but for our DSE1 plane. (d) Same as (b), but for our DSE1 plane. (e) Same as (a), but for our Muldrow plane. (f) Same as (b), but for our Muldrow plane. Color scheme and contours as in Figure 2. Distances are relative to AEIC DF event epicenter.

and H. C. Berg, vol. G-1 of *Geology of North America*, Geological Society of America, 1994.

Reasenber, P. A., and R. W. Simpson, Response of regional seismicity to the static stress change produced by the Loma Prieta earthquake, *Science*, 255, 1687–1690, 1992.

Richter, D. H., and N. A. Matson, Jr., Quaternary faulting in the eastern Alaska Range, *Bull. Geol. Soc. Am.*, 82, 1529–1540, 1971.

Savage, J. C., and M. Lisowski, Deformation in the Yakataga seismic gap, southern Alaska, 1980–86, *J. Geophys. Res.*, 93, 4731–4744, 1988.

Simpson, R. W., and P. A. Reasenber, Earthquake-induced static-stress changes on central California faults, in *The Loma Prieta, California, Earthquake of October 17, 1989 — Tectonic Processes and Models*, U.S. Geol. Surv. Prof. Pap. 1550-F, edited by R. W. Simpson, pp. F55–F89, U.S. Geological Survey, 1994.

Stein, R. S., The role of stress transfer in earthquake occurrence, *Nature*, 402, 605–609, 1999.

Wessel, P., and W. H. F. Smith, New, improved version of Generic Mapping Tools released, *EOS Trans. AGU*, 79, 579, 1998.

Table 1. Regional Faults Studied

Fault	Lat 1	Lon 1	Lat 2	Lon 2	L_{as} ^a	L_{dd} ^b	Strike	Dip	Rake	Ref.	ΔCFF ^c
Castle Mtn (NE)	61.90	-148.36	61.61	-150.00	92.3	25	251	70NW	160	1,2	10
Castle Mtn (SW)	61.61	-150.00	61.35	-151.04	62.2	25	245	70NW	160	1,2	< 10
Chugach-St. Elias	60.4	-141.5	60.5	-144.0	137.5	20	271	45N	90	1,3	-8
Cross Ck (CCNW)	62.31	-142.54	61.80	-141.83	68.1	20	143	90	180	1,4	420
Cross Ck (CCSE)	61.80	-141.83	61.53	-141.27	42.5	20	130	90	180	1,4	10
Denali (Muldrow)	63.49	-148.66	63.22	-151.10	125.4	20	258	90	180	1	80
Denali (DSE1)	62.64	-142.64	62.07	-140.69	119.6	20	118	90	180	1	470
Denali (DSE2)	62.07	-140.69	60.89	-138.08	190.5	20	126	90	180	1	20
Denali (TBC) ^d	63.22	-151.10	61.20	-158.20	431.7	20	245	90	180	1	< 6
Yakataga Gap	59.32	-141.36	59.43	-144.88	200	200	270	10N	105	1,3	-20

^aAlong-strike length, km

^bDown-dip width, km

^cMaximum absolute change, kPa

^dDenali fault, Tonzona-Boss Creek segments

Faults start at the surface. Coordinates are for updip edge of each fault. ΔCFF uncertainty ± 10 kPa. References: 1, *Plafker et al.* [1994]; 2, *Lahr et al.* [1986]; 3, *Savage and Lisowski* [1988]; 4, *Richter and Matson, Jr.* [1971]

Greg Anderson, U.S. Geological Survey, Pasadena CA 91106-3212 (ganderson@usgs.gov); Chen Ji, Seismological Laboratory, California Institute of Technology, Pasadena CA 91125

This preprint was prepared with AGU's L^AT_EX macros v5.01, with the extension package 'AGU++' by P. W. Daly, version 1.6b from 1999/08/19.